Research article

CFD simulation study and experimental analysis of indoor air stratification in an unventilated classroom: A case study in Spain

Carmela Concilio [a], Patricia Aguilera Benito [b,*], Carolina Piña Ramírez [c], Giacomo Viccione [d]

[a] *University of Salerno, Department of Civil Engineering, Fisciano, Italy*
[b] *Universidad Politécnica de Madrid, Departamento de Tecnología de La Edificación, Spain*
[c] *Universidad Politécnica de Madrid, Departamento de Construcciones Arquitectonicas y su Control, Spain*
[d] *Environmental and Maritime Hydraulics Laboratory (LIDAM), University of Salerno, Fisciano, Italy*

ARTICLE INFO

ABSTRACT

Health problems and respiratory diseases are associated with poor indoor air ventilation. We investigated the air quality inside a classroom-laboratory where no ventilation is provided. The case of study, consisting of an internal enclosure, is located at the Escuela Técnica Superior de Edificación (ETSEM) of Madrid (Spain). The high height favours air stratification which is analysed in terms of temperature and CO_2 spatial distribution. Temperature, air humidity, atmospheric pressure and CO_2 concentration measurements were taken in time at three different height locations. A CFD numerical model was established to analyse air quality. Flow circulation is derived by solving full 3D Navier – Stokes governing equations, coupled with the thermal problem. The diffusion problem of the CO_2 produced by the inner occupants is then derived from the kinematics solution. Three scenarios were taken into account: occupants seated (1), standing (2), half seated, half standing (3). Results clearly show the air stratification as a result of density gradient, which is in turn determined by temperature difference between the occupants and the surrounding air. Temperature prediction maximum relative error is contained to 3.5 %. As expected, CO_2 concentration increases over time, reaching maximum values depending on the configuration considered and height location.

Abbreviation	Term
$\Delta CO2$	Difference in CO2 concentration.
ACH	Air changes per hour
CO	Carbon Monoxide
CO2	Carbon dioxide
CTE	Technical Building Code, Spain
ETSEM	Escuela Técnica Superior de Edificación (Higher Technical School of Construction)
EN	European Standards
F	Statistical test F (Ronald Fisher)
HS	Basic documenton salubrity

(continued on next page)

---

* Corresponding author.
  E-mail address: patricia.aguilera@upm.es (P. Aguilera Benito).

(*continued*)

Abbreviation	Term
IAQ	Indoor Air Quality
IEQ	Indoor Environmental Quality
IEQcat	Indoor Environmental Quality category for design
NOX	Oxides of nitrogen
ns	Crowding index per unit area
O3	Ozone
OMS (WHO)	World Health Organization
p	Significance value
PM	Particulate Matter
ppm	parts per million
qB	ventilation rate for building materials
Qop	specific external air flow per person
qp	ventilation rate for people
qv	minimum flow for housing
SARS-CoV-2	Severe acute respiratory syndrome Coronavirus 2
SIMA	Italian Society of Environmental Medicine
SO2	Sulfur dioxide
UNE	Spanish Association for Standardisation
UNESCO	United Nations Educational, Scientific and Cultural Organization.
UNI	Italian national unification body

1. Introduction

Approximately 80 % of our time is allocated to indoor environments, rendering the surveillance of indoor air quality indispensable due to its direct correlation with human health [1].

Moreover, research has demonstrated that substandard indoor environmental quality is not only linked to health complications [2], but also to the deterioration of cognitive functions, leading to a reduction in productivity by as much as 50 % [3–6]. The importance of both indoor and outdoor air quality has been amplified and is garnering heightened attention in the wake of COVID-19 [7–13].

As per the UNE 171330:2008 standard, indoor air quality is characterized by the levels of chemical and microbiological contamination, in addition to the values of physical parameters such as temperature, humidity, acoustics, or luminescence. Contamination can originate from external air introduced into the building, or from internal sources such as occupancy, the type of activity conducted, furniture, construction materials, or combustion occurring indoors [14].

Given the substantial amount of time spent in indoor environments, there has been a progressive escalation in indoor CO_2 concentrations and associated health hazards. CO_2 levels exceeding 1000 parts per million (ppm) are correlated with diminished ventilation rates in classrooms, leading to a higher incidence of headaches, amplified inattentiveness, altered respiratory patterns, and an elevated probability of asthma attacks among students. Furthermore, suboptimal ventilation rates, reduced relative humidity, and elevated temperatures adversely impact the cognitive capabilities of students within classroom settings [15].

Furthermore, Goal 13 of the United Nations' 2030 Agenda for Sustainable Development mandates immediate measures to mitigate climate change and its planetary repercussions [16]. As per the International Energy Agency's reports, the construction sector is responsible for approximately 36 % of global carbon dioxide emissions, thereby positioning it as a pivotal component in the pursuit of environmental sustainability [17].

Conventional building energy models predominantly concentrate on energy efficiency and cost-effectiveness, potentially neglecting other parameters that could not only facilitate a reduction in consumption but also enhance the quality of life for occupants. In the context of indoor air quality, these traditional models have primarily focused on temperature, humidity, and particulates, often underestimating the role of CO_2 [18]. The importance of CO_2 in indoor air quality is multifaceted. Firstly, elevated levels of CO_2 can precipitate cognitive dysfunction and health complications. Secondly, CO_2 concentrations can serve as an indicator of the adequacy of ventilation within a building. Therefore, the incorporation of CO_2 into building energy models is vital for the attainment of sustainability objectives and the assurance of occupant health and comfort.

The study of CO_2 in indoor air quality presents a multitude of challenges. One of the primary challenges is the complexity of the models. Buildings are intricate systems exhibiting properties of nonlinearity, multicollinearity, and stochasticity. Another challenge is the requirement for cross-disciplinary knowledge and collaboration. It extends beyond understanding the physics of buildings to encompass the chemistry of CO_2 emissions and the economics of energy utilization. Moreover, real-time monitoring of CO_2 levels in indoor air quality necessitates the development of advanced cyber-physical systems [19].

Given the significance of indoor air quality, in conjunction with the prevailing climate crisis and the environmental footprint engendered by the energy consumption of the building sector, it is imperative to meticulously design systems predicated on specific needs. Furthermore, it is crucial to integrate energy conservation strategies with the objective of augmenting their efficiency and expediting their contribution towards decarbonization [20,21].

In light of the aforementioned factors, the surveillance of indoor air quality is of paramount importance. This research presents an opportunity to augment our comprehension of the impact of escalating energy efficiency standards, air quality, and mechanical ventilation, contingent upon the headroom of the enclosure.

Empirical evidence suggests that thermal stratification is a prevalent phenomenon in expansive living spaces during winter. This is attributed to natural buoyancy, which propels warmer, less dense air towards the ceiling. Typically, the relatively elevated temperature beneath the ceiling results in a substantial dissipation of heating energy [22–27]. This stratification has been described as one of the main causes of energy loss in buildings, so it is very important to take it into account when designing an installation [28–34].

Among various case studies, air infiltration emerges as the third most significant factor influencing energy consumption, accounting for 15–50 % of the annual energy expenditure for heating and cooling in commercial buildings within the United States [35]. Long-term CO_2 measurements have also been conducted, for instance, at an Australian college where data collected over an entire academic year averaged between 657 ppm and 2235 ppm [36–39]. Detailed analyses have been performed to understand how temperature stratification varies depending on different air-conditioning systems [30,40–42]. However, the stratification of CO_2 relative to occupants and effective practices to maintain satisfactory Indoor Air Quality (IAQ) is less understood. Few models in the current literature and practice consider dynamic occupancy behavior and indoor air quality. To address this gap, a dynamic indoor CO_2 model has been developed using machine learning algorithms to predict CO_2 concentrations over a range of prediction horizons. These systems are instrumental in conducting studies on building air conditioning to identify optimal energy savings and thermal efficiency, as well as to investigate the movement of particulate pollutants [43–46].

To the best of our knowledge, no existing study has conducted an in-depth examination of the coupled effects of thermal stratification on the dispersion of pollutants, CO_2, and humidity within a high-rise room. Consequently, the objective of this research is to ascertain the conditions of thermal stratification, CO_2 concentration, and humidity within a classroom-laboratory at the ETSEM School of Building Engineering, using field measurements. To this aim, a Computational Fluid Dynamics (CFD) model is developed the numerical solution of the coupled problem of heat transfer, laminar flow and transport of diluted species.

2. Methodology

2.1. Experimental method

2.1.1. Study case description

The classroom-laboratory under scrutiny serves as a venue for practical instruction, featuring seating arrangements for students in the center of the room. The room can accommodate up to 80 seated individuals. The classroom is equipped with models and simulators displayed on all its walls, facilitating the practical components of the courses and subjects imparted. It is situated on the basement floor −1 of the Escuela Técnica Superior de Edificación (ETSEM) in Madrid, Spain. The dimensions of the classroom-laboratory are 15 m (length) × 15 m (width) × 6 m (height). A distinguishing characteristic of the classroom is its considerable free height from the floor to the ceiling. (Fig. 1).

The classroom is an interior enclosure, surrounded by other classrooms around its perimeter. For this reason, it has no windows or grilles to the outside for natural ventilation. It has no mechanical or natural ventilation system. It is therefore of interest to analyse the indoor air quality in this room.

More specifically, owing to its tall 6-m height, it is interesting to analyse the stratification of the variables: temperature, humidity, pressure and CO_2 concentration.

2.1.2. Measuring system and sensors adopted

Brand new and factory-calibrated sensors for collecting data on temperature, relative humidity, air pressure and CO_2 concentration

Fig. 1. Classroom-Laboratory under study. Left. Photo during a master class. Right. Infographic of the classroom with a 3-m-high section.

were installed. The sensors were supplied by PCE Iberica S.L. Instrumentation dedicated to measurement, regulation, laboratory and weighing. The technical characteristics of the equipment can be seen in Table 1.

The sensors have been placed at the midpoint of one of the sides. About 7 m from the access to the classroom. It is a strategic point for analysis, as it is not only a place where students are seated, but also a transit point to access the classroom.

To analyse indoor air stratification, 3 sensors have been placed at different heights. Sensor number 1 is located 1.10 m above the floor, sensor number 2 at 2.90 m above the floor and sensor number 3 at 4.70 m above the floor (Fig. 2).

The data collection period for this study spanned from May 15, 2022, to June 15, 2022. Throughout this timeframe, the classroom environment varied significantly due to different operational states.

There were specific days when the school was not operational, and consequently, the classroom was unoccupied with all equipment powered down. These non-operational days were May 15, 21, 22, 28, 29, and June 4, 5, 11, 12.

On certain days, the classroom-laboratory remained open despite being unoccupied. During these periods, only the maintenance technician was present, and minimal lighting was maintained. The use of simulators or any other electrical equipment was not recorded on these days.

Finally, there were eight specific days when the classroom was fully operational due to a course being conducted for 20 participants. On these days, all necessary equipment and lighting systems were activated. These operational days were May 18, 19, 25, 26, and June 7, 8, 24, 25. This variation in operational states provides a unique perspective on energy usage patterns in an educational setting (Table 2).

2.2. Numerical method

2.2.1. Physical model

A 3D CFD numerical model, FEM based, was developed to simulate velocity field, pressure, unsteady temperature distribution and CO_2 concentrations for the inner air. The commercial solver COMSOL Multiphysics v 6.1 was used for this aim [47]. The solver allowed coupling three physical phenomena: heat transfer, laminar flow and transport of diluted species. The computational domain of the classroom-laboratory was generated as a closed box with insulated and impermeable walls and without a ventilation system. Domain was discretized using unstructured tetrahedral grid. The maximum element size is 0.9 m whereas the minimum allowed size is 0.27 in order to prevent the generation of many elements around small curved parts of the geometry; the maximum rate at which the element size can grow from a region with small elements to a region with larger elements was set to 1.5, so the element size can grow by at most 50 % (approximately) from one element to another. A boundary layers mesh with dense element distribution in the normal direction along no-slip boundaries was set (2 layers, thickness 0.5 m).

A grid convergence analysis was conducted by testing two mesh cases with 28128 and 346434 elements, respectively. The maximum local temperature difference was found to be 0.005 °C. This indicates that the results are convergent and do not vary significantly with increased mesh resolution. The convergence analysis by reducing the relative difference in temperatures is also adopted for Case 4 of Annex C of UNI EN ISO 10 211 [49].

2.2.2. Numerical details and boundary conditions

Fluid dynamics was coupled with heat transfer, because flow occurred naturally due to temperature gradients. The pressure p and

Table 1
Technical specifications of the sensors.

| TECHNICAL SPECIFICATIONS OF THE SENSORS	
Temperature	
Range	0 … +50 °C
Resolution	0,1 °C
Accuracy	±0,15 °C @ 0 … +20 °C
	±0,1 °C @ +20 … +50 °C
Air humidity	
Range	0 … 100 % H.r.
Resolution	0,1 % H.r.
Accuracy	±1,5 % H.r. @ 0 … 80 % H.r.
	±2 % H.r. @ 80 … 100 % H.r.
Atmospheric pressure	
Range	300 … 2000 hPa
Resolution	0,1 hPa
Accuracy	±2 hPa @ 25 °C y 750 … 1100 hPa
	±4 hPa @ 0 … +50 °C y 300 … 1200 hPa
CO2 concentration	
Range	0 … 40 000 ppm
Resolution	1 ppm
Accuracy	±(30 ppm + 3 % del valor) @ 400 … 10 000 ppm @25 °C
	±(6 … 10 % del valor) @ 0 … 400 ppm o 10 000 … 40 000 ppm
Temperature stability	2,5 ppm/°C @ T = 0 … 50 °C, 400 … 10000 ppm
Sensor type	NDIR sensor
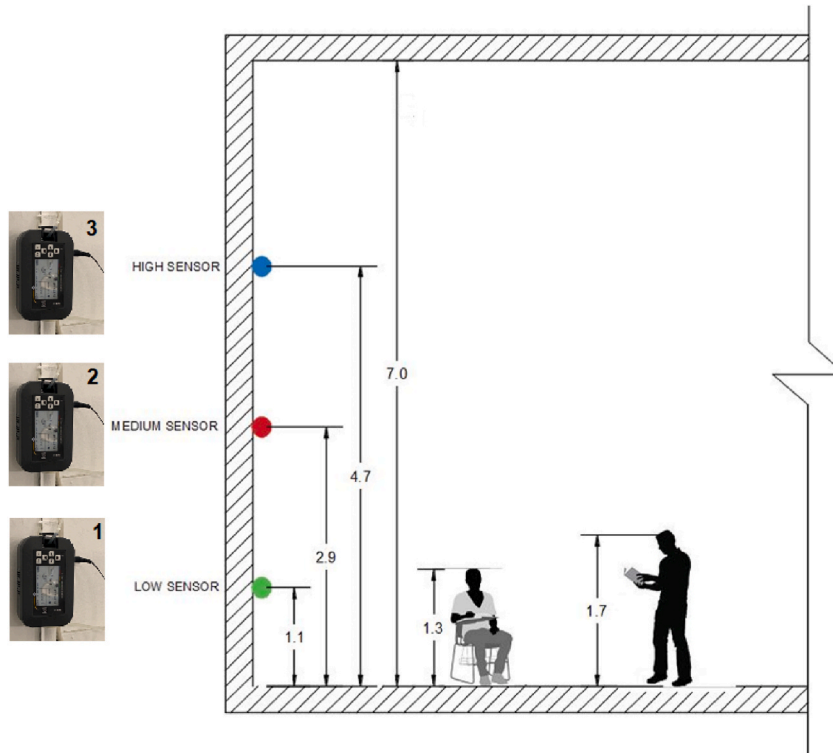
Fig. 2. Location of the sensors in the Classroom-Laboratory.

Table 2
Classroom-laboratory monitoring Calendar.

	SUN	MON	TUE	WED	THU	FRI	SAT	
MAY	15	16	17	18	19	20	21	
	22	23	24	25	26	27	28	
	29	30	31	1	2	3	4	JUNE
	5	6	7	8	9	10	11	
	12	13	14	15				

▨	Classroom-Laboratory closed
▨	Classroom-Laboratory with course for 20 people
▨	Open Classroom-Laboratory with only technical maintenance personnel

the velocity components u, v, w are the solution of the Navier-Stokes equations, while the temperature T is solved through the heat equation. Conjugate heat transfer was simulated by imposing [18] the following set of equations:

$$\rho C_p \frac{\partial T}{\partial t} + \rho C_p\, u \bullet \nabla T + \nabla \bullet (-k\nabla T) + \tau\, S - \frac{T}{\rho}\left(\frac{\partial \rho}{\partial T}\right)_p \left(\frac{\partial p_a}{\partial t} + u \bullet \nabla p_a\right) = Q \tag{1}$$

$$\rho\left(\frac{\partial u}{\partial t}+(u \bullet \nabla)u\right)= -\nabla p+\nabla \bullet \left[\mu\left(\nabla u+(\nabla u)^T\right)-\frac{2}{3}(\nabla \bullet u)I\right]+F \tag{2}$$

where $\rho = \rho(p, T)$ is the varying density (compressible flow), $\mu = \mu(T)$ is the dynamic viscosity, $k = k(T)$ is the thermal conductivity, F is the buoyancy force. The hydrodynamic and temperature fields were required inputs to estimate concentrations c of the n diluted species by imposing following equations:

$$\frac{\partial c}{\partial t}+\nabla \bullet J+u \bullet \nabla c = R \tag{3}$$

$$J= -D\nabla c \tag{4}$$

For each diluted species it was necessary to define concentration variable, diffusion coefficient $D\left[\frac{m^2}{s}\right]$, initial value and flow $J\left[\frac{mol}{m^2 s}\right]$ relative to the equivalent section.

Fig. 3 illustrates the model geometry. Twenty students were placed following the classic pattern of desks in classrooms.

The domain was bounded by impermeable walls. The applied no-slip condition resulted in zero velocity at the walls and in correspondence with inner occupants (cylinder objects in Fig. 3). Since in a cavity surrounded by walls system, pressure level is not uniquely determined, the pressure was fixed at a point to set a boundary condition for this variable [48].

In order to determine the occurrence of turbulent or laminar flow according to specific critical value, Grashof number was estimated because it is a measure of the buoyancy with respect to the viscous forces:

$$Gr=g\,\beta_\infty\left(T_w-T_\infty\right)\frac{L_{ref}^3}{\nu^2}$$

where g is the gravity acceleration [m s $^{-2}$], $\beta_\infty = $ is thermal expansion coefficient [K^{-1}], T_w is cylinder temperature [K], T_∞ is air temperature, L_{ref} is average reference length [H$_c$] of the hot cylinder [m], ν is kinematic viscosity [m^2 s $^{-1}$]. When external convection is induced by the temperature difference between the solid body (cylinder) surrounded by the air filling the cavity, the Grashof number was estimated using the average temperatures of the hot body (Tw = 37 °C) and the air (T_∞ = 20 °C). For a vertical cylinder, the height is the appropriate characteristic length because the heated air near the surface of the cylinder tends to rise, creating a velocity and
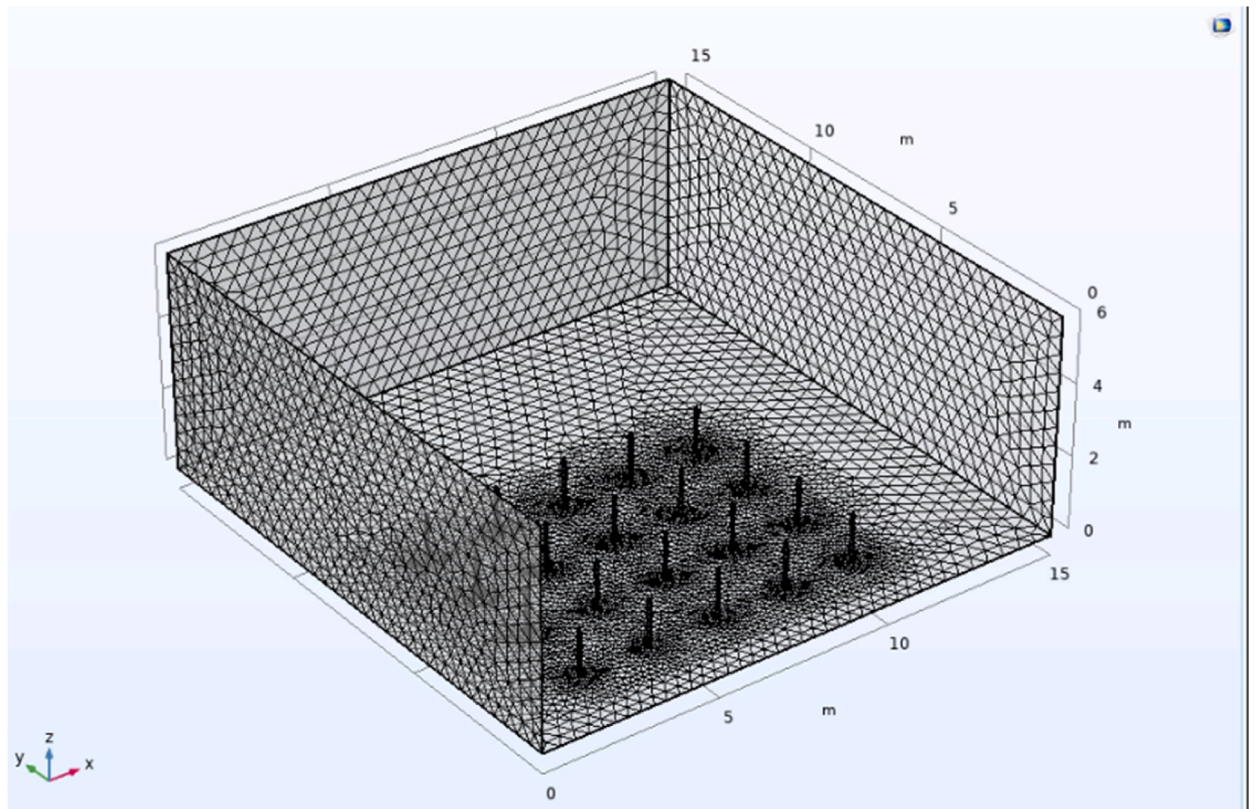

Fig. 3. The adopted mesh, consisting of an unstructured tetrahedral grid.

temperature profile that extends along the height of the solid. Furthermore, the temperature difference between the cylinder and the fluid causes a vertical density gradient, which in turn induces vertical convective motion. Finally, many empirical correlations for calculating the Nusselt number in natural convection for vertical cylinders are based on the height of the cylinder. In this case, the reference length was taken to be the height of the cylinder in the configuration in which the occupant is seated. Air properties were evaluated at 29 °C, being the average temperature between warm body and the cold fluid. This expression is useful for calculating the Rayleigh number, which remains below 10^9, allowing turbulence in the room to be neglected. The laminar flow and heat transfer interfaces have been fully coupled.

Temperature evolution during a period of 8 h was simulated, coincident with students' occupancy. According to the European standard, inner thermal loads are counted as constant heat sources estimated as 80 W/m^2 for student, counted as metabolic energy. People have been modelled like cylinders, whose thermo-physical properties are similar to those of water. Edges of the adopted simplified objects representing the occupants, consist of higher-than-ambient-temperature sources in a cavity. Temperature drop produces density variation that drives the buoyant flow. According to Boussinesq's term, it was set a volume force proportional to the temperature difference between hot surfaces and the inner air, both monitored by numerical contour and domain probes, respectively.

Similar to the convective problem, a source of CO_2 was considered on the top of cylinders. Emitted carbon dioxide depends on the frequency and volume of breaths, as well as the person's metabolism and environmental conditions. In general, the breathing rate of an adult at rest is about 12–20 breaths per minute, and the average volume of each breath is about 0.5 L. According to the percentage of CO_2 in the exhaled air (4 % of 0.5 l), the average respiration rate (3 s), and the evaluated equivalent exchange area (1 m^2), a constant flux of $1.82 \bullet 10^{-4}$ $mol\ m^{-2}s^{-1}$ was estimated to simulate CO_2 diffusion. It was necessary to consider the molar volume of the pollutant as the temperature and pressure is time dependent.

2.2.3. Adopted simulation scenarios

Three configurations were set up: two scenarios consider that all occupants are seated or standing, arranged in a 4 × 5 rectangular grid. Based on body surface area and height (H_c), the latter assumed 1.70 m for standing configuration and 1.30 m for seated configuration, the radius (R) of the equivalent heat source was calculated, see Table 3. The third assumed configuration assumes half of the occupants standing, half seated in the room, see Table 4.

3. Results and discussion

3.1. Field results, experimental part

The objective of this study is to analyse the indoor air quality and the stratification behavior of a classroom-laboratory. This analysis is conducted through the measurement of four key variables: temperature (in °C), relative humidity (in %), atmospheric pressure (in hPa), and CO_2 concentration (in ppm).

Stratification is a well-documented thermal phenomenon that occurs within enclosed spaces, driven by the differential densities of warm and cold air. The less dense warm air tends to ascend towards the upper regions of the space, displacing the denser cold air towards the lower regions. This stratification effect is evidenced by the temperature readings from sensors placed at different heights within the room. The sensor at the top (represented by the blue line) records the highest temperatures, while the sensor at the bottom (represented by the green line) records the lowest temperatures.

Furthermore, during periods when the classroom is occupied by 20 individuals (indicated by the green bands), the highest temperature values are observed. This data provides an opportunity to examine the variation in temperature during active class sessions and the subsequent drop in temperature during mid-day breaks. This analysis contributes to a comprehensive understanding of the thermal dynamics within an occupied educational setting (Fig. 4).

Relative humidity stratification refers to the vertical distribution of the amount of water vapour in the atmosphere as a function of height above ground level.

For relative humidity, the opposite is true as for temperature. The highest values are recorded at the sensor located at the bottom and the lowest humidity values are recorded at the sensor located at the top of the classroom-laboratory (Fig. 5). It can be stated that it manifests itself cyclically in the opposite direction to temperature variations, since the higher the temperature, the less humidity. Furthermore, it is observed that the relative humidity values are not close to 100 %, so condensation cannot occur on the surfaces, which would cause problems with mold, corrosion, rot and other deterioration related to humidity.

The atmospheric pressure measured by the three sensors is the same, regardless of the height at which they are placed. The pressure in the classroom-laboratory is between 936 ppm and 954 ppm (Fig. 6), which represents acceptable values in temperate regions.

Regarding CO_2 concentration, it is interesting to note that the highest concentrations are found in the sensor placed at a medium height, with a difference with respect to the sensor placed at the top and at the bottom of up to 400 ppm (Fig. 7). However, no measurement shows high concentrations of CO_2, since particularly when it is above 1000 ppm, it causes numerous negative effects on

Table 3
Geometric equivalent parameters.

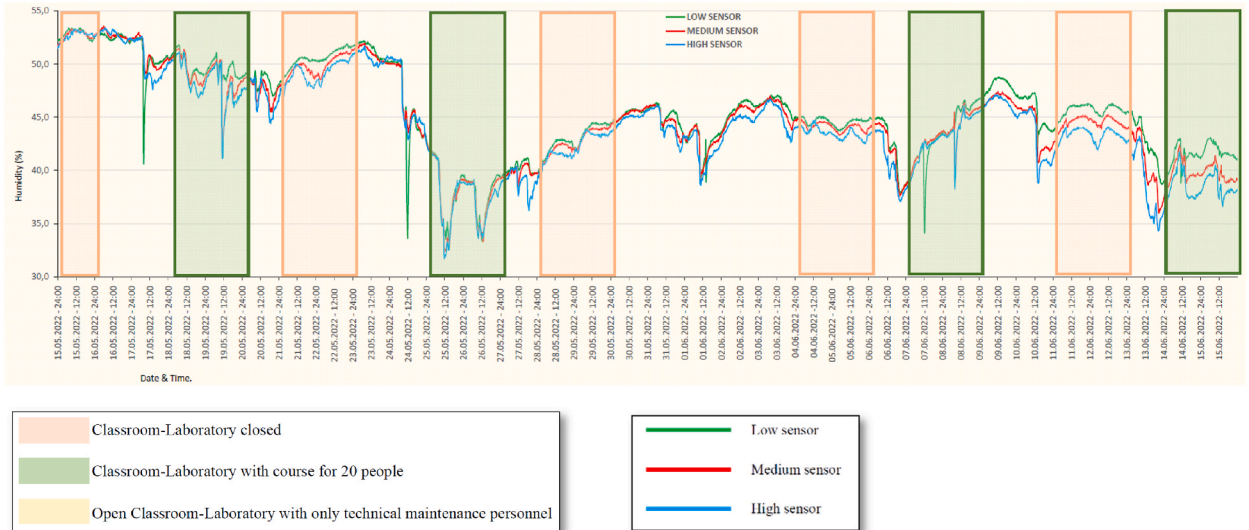| Geometric equivalent parameters	Standing	Seated
Hc [m]	1.30	1.70
R [m]	0.19	0.15

Table 4
Simulated scenarios.

Configurations	N° students	
	Standing	Seated
1	0	20
2	20	0
3	10	10
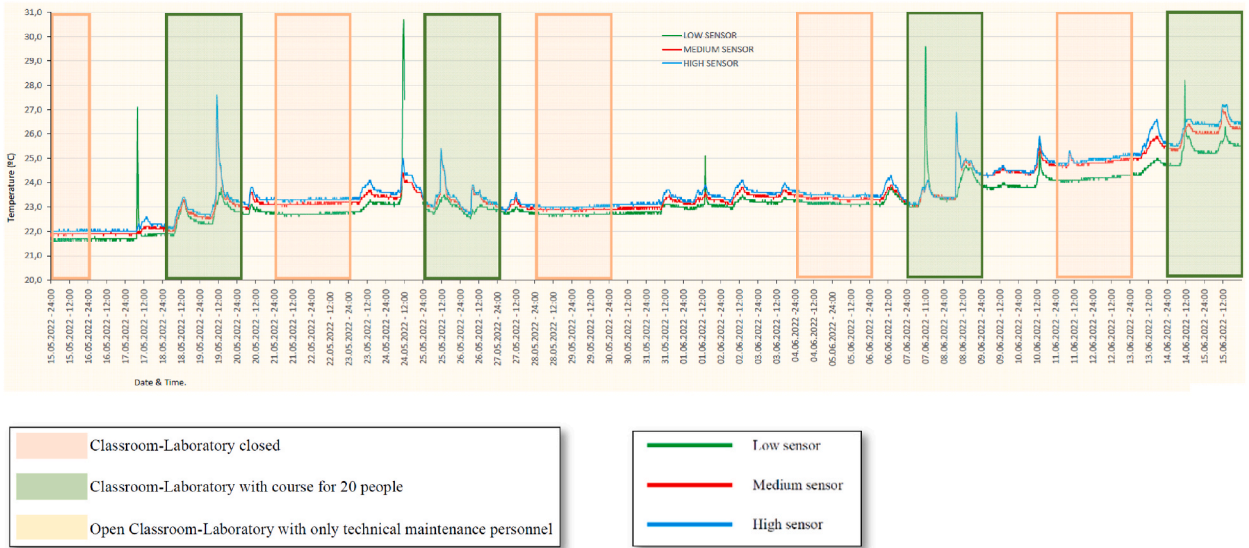
Fig. 4. Temperature graph (°C) during the analysis period.

Fig. 5. Relative humidity graph (%) during the analysis period.

people's health in the short and long term such as respiratory diseases and reduced lung capacity.

3.2. Simulation results

The model simulated the effect of 20 occupants inside the room during the day 2022/05/18 from 7 a.m. to 3 p.m., when laboratory
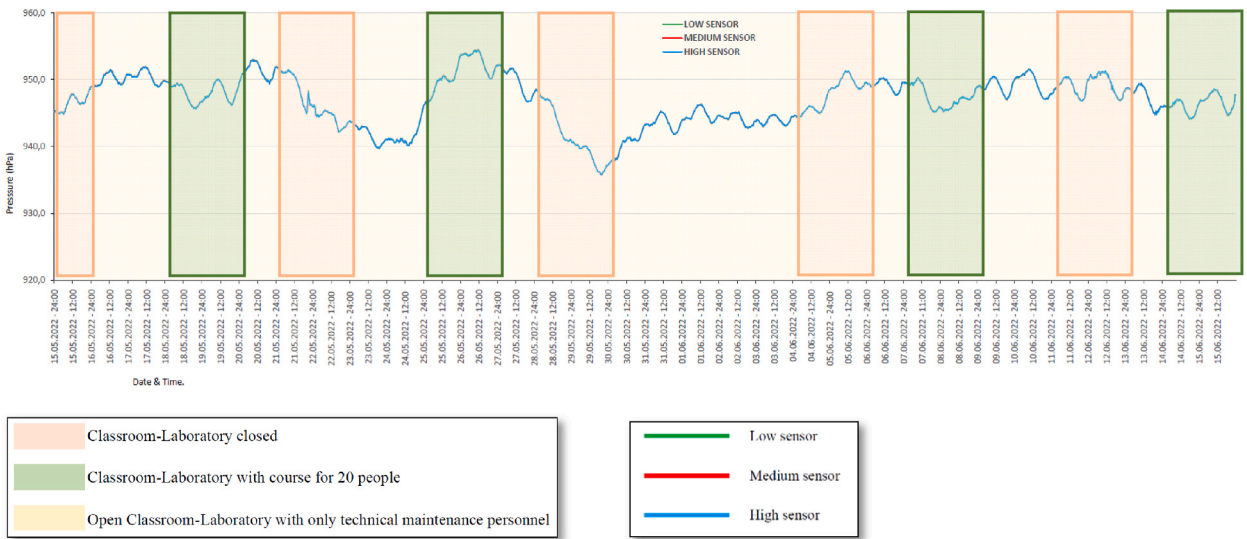
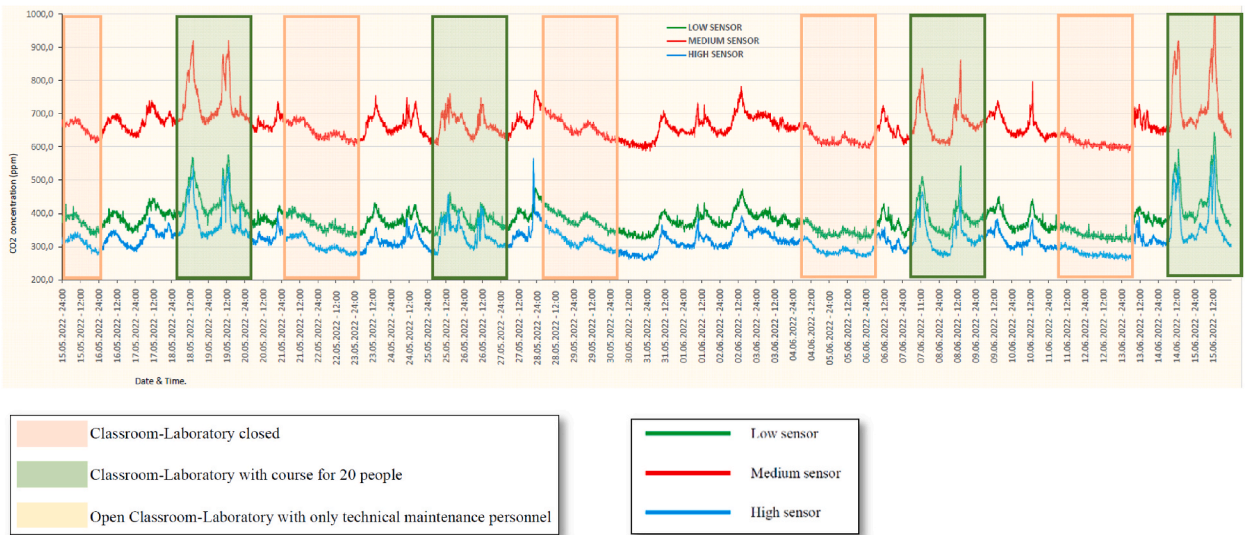**Fig. 6.** Atmospheric pressure graph (hPa) during the analysis period.

Fig. 7. Graph of CO_2 concentration (ppm) during the analysis period.

was effectively occupied for a lesson. In order to compare experimental data and numerical results, the configuration with all occupants seated is next considered.

The finite element analysis returned the temperature of the indoor environment, the velocity field and the concentration of CO_2 inside the cavity.

Fig. 8 represents air velocity inside the laboratory during the analysis period. Velocity increases with time and is greatest near the occupants, where the buoyancy forces are higher. The difference in air density triggers convective motions, even though the velocities are low in magnitude, as expected. The fluid flow occurs in the form of a large recirculation loop [20].

Speed range does not seem to have changed significantly from scenario 1 to 3.

Students, who have an initial temperature higher than air's, resulted in an average temperature increase of two degrees in 8 h, estimated by means of fluid domain probe. In addition, three numerical probes were positioned in the fluid domain at the same hight of the temperature sensors.

Natural air recirculation tends to equalise the temperature in the room in 8 h. However, stratification due to the density difference is visible, as shown by the Ti evolutions in Table 5 and Fig. 9. Therefore, the highest temperatures are detected by the probe at 4.7 m. The curves of Fig. 9, quantitatively displayed in Table 6 for selected points, show that the numerical solution matched the experimental data. Suggested model tends to overestimate the inner temperature, especially in the final phase of the period considered, but the
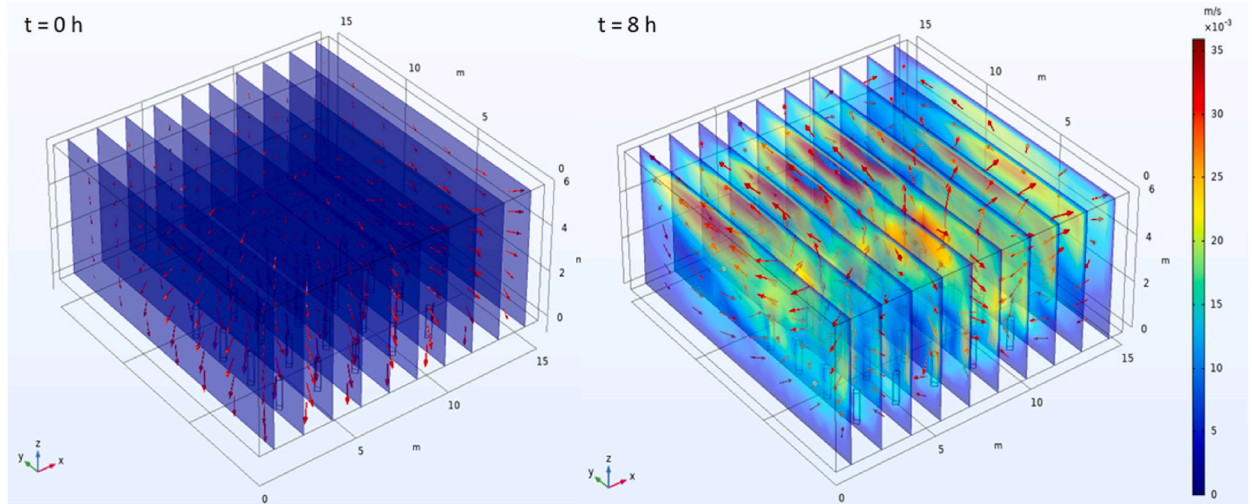
Fig. 8. Velocity field inside the cavity (configuration 1).

maximum relative error is generally contained within the 3.5 %.

Table 6 shows the relative error between the experimental data and the numerical results e, in percent. The data obtained belong to configuration 1.

The finite element analysis returned the temperature and pressure of the indoor environment, consequently, allowed to calculate CO_2 molar volume; the instantaneous concentration of pollutant can be immediately obtained.

Fig. 10 depicts 4 horizontal section planes of the laboratory with seated students. The model did not consider any ventilation, so the pollutant accumulates towards the walls surrounding the students.

Tables 7 and 8 shows the average indoor ambient temperature for the selected times and positions for both configuration 2 and 3.

In good agreement with the experimental data collected, the highest CO_2 concentrations are found at an average height of 1.1–2.9 m, where students are present. The greater value reached is around 1101 ppm, being recorded in the occupied area at 1.30 m, while the lowest value at the same hight above the floor, is 326 ppm after 8 h. Into fluid domain, the average concentration value after analysis period is 535 ppm.

Fig. 11 shows the numerical model with the distribution of CO_2 concentration (ppm) for different heights (m) above the ground after 8 h.

Tables 9–11 below show average, minimum and maximum values of the CO_2 concentration for given floor heights and for selected times according to the other proposed configurations (mean value was calculated integral on section plane).

According to the results given in the above Tables, there is the formation of thermal stratification in the room, whereby the internal temperature only varies along the height of the room and increases over time, since the active sources are limited during the investigation period. Consequently, the differences in the heat source distribution are negligible. The inner temperature does not seem to change significantly, considering the three scenarios.

On the other hand, the CO_2 concentration is not uniform in the x-y plane, reaching high values in the most fully loaded zone. In line with the recorded values of the velocity field, the buoyancy forces fail to even and smooth out the concentration in the horizontal plane. Furthermore, there is no upward stratification of pollutants, but the concentration is highest at the level of the human sources. As it can be seen, the concentration increases over time and cumulates, as expected, in the head zone. The highest value is recorded by the second sensor, considering that the people are all standing, while for the mixed configuration, the first sensor detects the maximum one.

In order to design a correct air-conditioning system, it usually requires the involvement of specific software and algorithms that are more cumbersome and expensive to purchase. Within this context, a simple and easy-to-handle, yet accurate, thermal model to evaluate the unsteady thermal and fluid dynamics response of inner air was developed. However, it is important to emphasise that this model takes into account a single load (both for heat and CO_2) due to the presence of occupants.

Further developments of the present work are intended to include effects of the thermal and ventilation plants and the introduction

Table 5
Inner average temperature (configuration "seated").

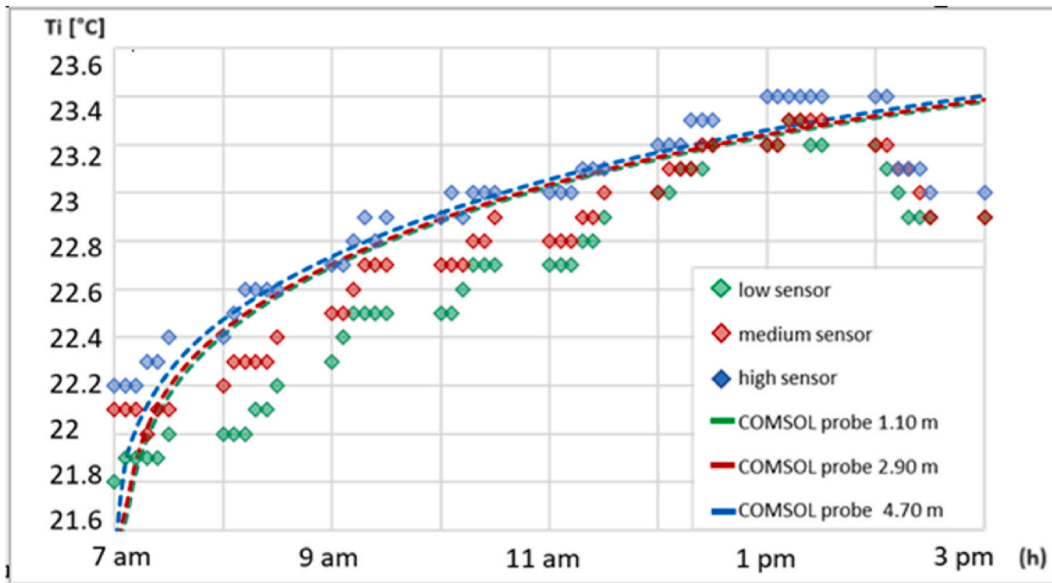| time position	9 a.m. Ti [°C]	11 a.m. Ti [°C]	1 p.m. Ti [°C]	3 p.m. Ti [°C]
1.1 m	22.69	23.02	23.23	23.37
2.9 m	22.70	23.03	23.24	23.39
4.7 m	22.74	23.06	23.26	23.40

Fig. 9. Inner temperature during the analysed period: comparison with experimental data (configuration 1).

Table 6
Relative error between experimental data and numerical results (configuration 1).

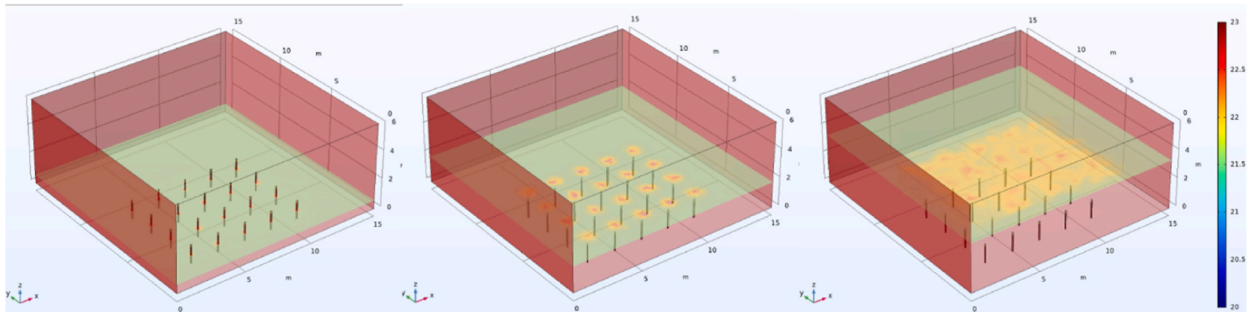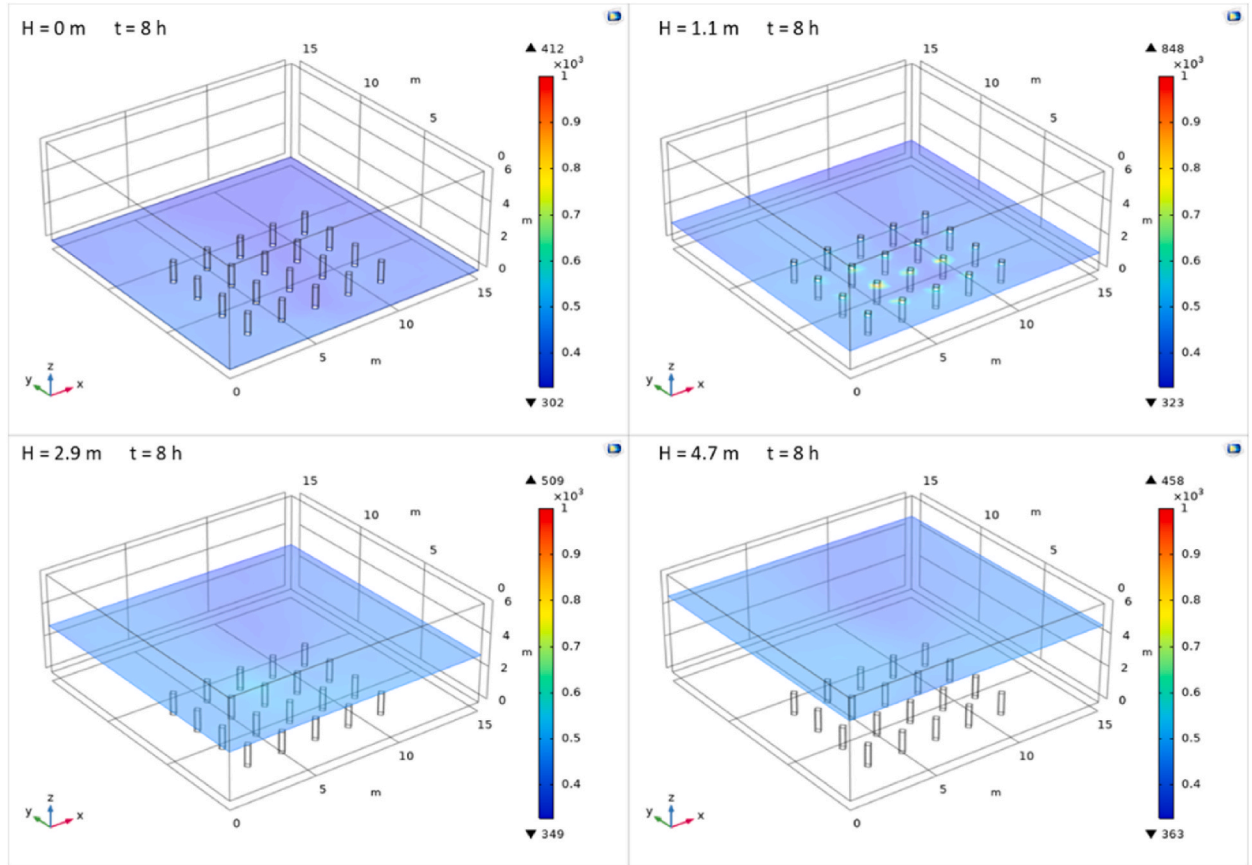| time position	9 a.m. [%]	11 a.m. [%]	1 p.m. [%]	3 p.m. [%]
1.1 m	0.72	2.24	0.14	2.08
2.9 m	0.40	0.89	0.18	2.13
4.7 m	0.02	0.76	0.86	1.76

Fig. 10. Temperature CFD results on different heights (configuration 1).

Table 7
Indoor environment average temperature for selected times and positions (configuration 2).

time position	9 a.m. Ti [°C]	11 a.m. Ti [°C]	1 p.m. Ti [°C]	3 p.m. Ti [°C]
1.1 m	22.77	23.01	23.13	23.24
2.9 m	22.76	23.02	23.14	23.25
4.7 m	22.80	23.04	23.16	23.27

Table 8
Indoor environment average for selected times and positions (configuration 3).

time position	9 a.m. Ti [°C]	11 a.m. Ti [°C]	1 p.m. Ti [°C]	3 p.m. Ti [°C]
1.1 m	22.80	22.98	23.06	23.09
2.9 m	22.81	22.99	23.07	23.10
4.7 m	22.84	23.00	23.09	23.12

Fig. 11. Numerical model: CO_2 concentration distribution (ppm) for different heights above the floor after 8 h.

Table 9
Maximum and minimum values of CO_2 concentration for selected times and positions (configuration 1).

time position	9 a.m. [ppm]			11 a.m. [ppm]			1 p.m. [ppm]			3 p.m.		
	C_{min}	C_{max}	C_{ave}	C_{min}	C_{max}	C_{ave}	C_{min}	C_{max}	C_{ave}	C_{min}	C_{max}	C_{ave}
1.1 m	40	245	215	99	428	377	215	612	435	323	848	629
2.9 m	43	113	98	113	268	234	238	395	276	349	509	457
4.7 m	46	102	82	118	248	201	251	364	271	363	458	424

Table 10
Maximum and minimum values of CO_2 concentration for selected times and positions (configuration 2).

time position	9 a.m. [ppm]			11 a.m. [ppm]			1 p.m. [ppm]			3 p.m.		
	C_{min}	C_{max}	C_{ave}	C_{min}	C_{max}	C_{ave}	C_{min}	C_{max}	C_{ave}	C_{min}	C_{max}	C_{ave}
1.1 m	34	70	53	86	133	123	136	186	177	204	243	225
2.9 m	40	90	63	101	163	117	152	210	169	211	264	248
4.7 m	41	78	59	106	141	129	156	199	166	214	254	240

Table 11

Maximum and minimum values of CO_2 concentration for selected times and positions (configuration 3).

time position	9 a.m. [ppm]			11 a.m. [ppm]			1 p.m. [ppm]			3 p.m.		
	C_{min}	C_{max}	C_{ave}	C_{min}	C_{max}	C_{ave}	C_{min}	C_{max}	C_{ave}	C_{min}	C_{max}	C_{ave}
1.1 m	14	243	231	50	300	248	71	354	302	89	449	395
2.9 m	17	104	74	54	145	89	81	206	136	97	271	239
4.7 m	36	86	63	59	132	120	86	190	152	101	250	212

of random thermal loads that create more realistic boundary conditions.

4. Conclusion

In this work, the air quality of a laboratory classroom with a singular characteristic, which is the height of the room, was investigated experimentally and numerically, giving the option to analyse the air stratification in detail.

For this purpose, 3 sensors were installed at different heights during the months of May and June and a 3D CFD model was also built. The numerical results were compared with available measurements of temperature, air humidity, atmospheric pressure, and CO_2 concentration, showing in general a satisfactory agreement.

The results clearly show the stratification of the air because of the density gradient, which in turn is determined by the temperature difference between the occupants and the surrounding air.

The temperature has its maximum values in the upper part of the classroom, and in the simulation we have obtained that the maximum relative error of temperature prediction is contained in 3.5 %. Relative humidity is the opposite of temperature, with its highest values in the lower part of the classroom.

As expected, the CO_2 concentration increases with time, reaching maximum values depending on the configuration considered and the location in height. It is important to mention that the part where the highest CO_2 concentrations are collected is the intermediate sensor.

This study sheds light on the air stratification inside the classroom, providing valuable information on the distribution of temperature, humidity, and CO_2 at different heights. The agreement between numerical simulation and measurements demonstrates the reliability of this tool for further analysis and optimisation of indoor air quality in such environments. This research provides relevant information that can contribute to a better understanding and design of indoor spaces, ensuring healthier and more comfortable conditions for their occupants.

Data availability

Data will be made available on request.

CRediT authorship contribution statement

Carmela Concilio: Software, Resources, Methodology. **Patricia Aguilera Benito:** Formal analysis, Conceptualization. **Carolina Piña Ramírez:** Validation, Project administration, Investigation. **Giacomo Viccione:** Writing – review & editing, Supervision, Resources, Funding acquisition.

Declaration of competing interest

The authors declare that they have no known competing financial interests or personal relationships that could have appeared to influence the work reported in this paper.

Acknowledgments

References

[1] E. Yarke, Ventilación natural de edificios : fundamentos y métodos de cálculo para aplicación de ingenieros y arquitectos, Nobuko, Buenos Aires, 2005.

[2] E. Lepore, P.A. Benito, C.P. Ramírez, G. Viccione, Indoors ventilation in times of confinement by SARS-CoV-2 epidemic: a comparative approach between Spain and Italy, Sustain. Cities Soc. 72 (June) (2021) 103051, https://doi.org/10.1016/j.scs.2021.103051.

[3] S. De Ventilación, et al., Sistemas de ventilacion y estudio de la monitorización por sensores de CO2 en edificio CIHEAM, 2021.

[4] M.A.T. Bainotti, IAQ-UPC - Diagnostico de la calidad del aire interior en el ámbito universitario de la UPC_Campus Sur, 2017.

[5] P. Córdova-mendoza, Primera caracterización de emisiones contaminantes y la calidad del aire en Ica, Perú, Rev. Cubana Quím. 33 (1) (2021) 138–153 [Online]. Available: file:///C:/Users/Godoy/Desktop/Primera caracterización de emisiones contaminantes y calidad del aire en Ica.pdf.

[6] P. Aguilera Benito, C. Piña Ramírez, G. Viccione, E. Lepore, Ventilation for residential buildings: critical assessment of standard requirements in the COVID-19 pandemic context, Front. Built Environ. 7 (August) (2021) 1–10, https://doi.org/10.3389/fbuil.2021.656718.

[7] W. Ming, X. Wang, Y. Wang, The intersection of COVID-19 and air pollution : a systematic literature network analysis and roadmap for future research, Environ. Res. 237 (P2) (2023) 116839, https://doi.org/10.1016/j.envres.2023.116839.

[8] G. Ozler, H. Grosshans, Airborne virus transmission : increased spreading due to formation of hollow particles, Environ. Res. 237 (P2) (2023) 116953, https://doi.org/10.1016/j.envres.2023.116953.

[9] T. Alexandru, B. Marinela, D. Laura, B. Irina, Mechanical and environmental performances of concrete using recycled materials, Procedia Manuf. 32 (2019) 253–258, https://doi.org/10.1016/j.promfg.2019.02.211.

[10] D. Mihăilă, et al., Air quality changes in NE Romania during the first Covid 19 pandemic wave, 1–16, Heliyon 9 (8) (2023) e18918, https://doi.org/10.1016/j.heliyon.2023.e18918.

[11] C. Konstantinou, et al., Assessment of indoor and outdoor air quality in primary schools of Cyprus during the COVID–19 pandemic measures in May–July 2021, Heliyon 8 (5) (2022) e09354, https://doi.org/10.1016/j.heliyon.2022.e09354.

[12] C.H. Yu, S.C. Chang, E.C. Liao, Is the excellent air quality a protective factor of health problems for Taitung County in eastern Taiwan? Perspectives from visual analytics, Heliyon 9 (3) (2023) e13866, https://doi.org/10.1016/j.heliyon.2023.e13866.

[13] O. Atiaga, et al., Assessment of variations in air quality in cities of Ecuador in relation to the lockdown due to the COVID-19 pandemic, Heliyon 9 (6) (2023) e17033, https://doi.org/10.1016/j.heliyon.2023.e17033.

[14] AENOR, UNE 171330-01 Calidad Ambiental en Interiores, 2008, pp. 1–2.

[15] S. Hama, P. Kumar, A. Tiwari, Y. Wang, P.S. Linden, The underpinning factors affecting the classroom air quality, thermal comfort and ventilation in 30 classrooms of primary schools in London, Environ. Res. 236 (P2) (2023) 116863, https://doi.org/10.1016/j.envres.2023.116863.

[16] J. Navarro, Agenda 2030 en el Objetivo Desarrollo Sostenible 6: Agua limpia y Saneamiento, Curso Deontol. Prof. del Semest 2020 (2020) 1–247 [Online]. Available: https://repositorio.ulcb.edu.pe/handle/ULCB/252.

[17] J.M. Rey-Hernández, J.F. San José-Alonso, E. Velasco-Gómez, C. Yousif, F.J. Rey-Martínez, Performance analysis of a hybrid ventilation system in a near zero energy building, Build. Environ. 185 (Nov) (2020), https://doi.org/10.1016/j.buildenv.2020.107265.

[18] R.A. González-Lezcano, S.K. Sansaniwal, Editorial: healthy and energy efficient buildings, Front. Built Environ. 9 (November) (2023) 2021–2024, https://doi.org/10.3389/fbuil.2023.1341133.

[19] T. Circle, et al., ASHRAE Position Document on, 2020.

[20] B. Dai, Y. Tong, Q. Hu, Z. Chen, Characteristics of thermal stratification and its effects on HVAC energy consumption for an atrium building in south China, Energy 249 (2022), https://doi.org/10.1016/j.energy.2022.123425.

[21] G. Swamy, Development of an indoor air purification system to improve ventilation and air quality, Heliyon 7 (10) (2021) e08153, https://doi.org/10.1016/j.heliyon.2021.e08153.

[22] G. Wei, et al., A review and comparison of the indoor air quality requirements in selected building standards and certifications, Build. Environ. 226 (October) (2022) 109709, https://doi.org/10.1016/j.buildenv.2022.109709.

[23] X. Zhang, C. Zhao, T. Zhang, J. Xie, J. Liu, N. Zhang, Association of indoor temperature and air quality in classrooms based on field and intervention measurements, Build. Environ. 229 (December 2022) (2023) 109925, https://doi.org/10.1016/j.buildenv.2022.109925.

[24] J. Hu, Y. Kang, J. Yu, K. Zhong, Numerical study on thermal stratification for impinging jet ventilation system in office buildings, Build. Environ. 196 (March) (2021) 107798, https://doi.org/10.1016/j.buildenv.2021.107798.

[25] H. Wang, P. Zhou, C. Guo, X. Tang, Y. Xue, C. Huang, On the calculation of heat migration in thermally stratified environment of large space building with sidewall nozzle air-supply, Build. Environ. 147 (October 2018) (2019) 221–230, https://doi.org/10.1016/j.buildenv.2018.10.003.

[26] X. Huang, L. Gao, Impacts of the side ratio of isolated buildings on airflows and pollutant dispersion under different temperature stratifications : numerical investigations, 0–1 27 (4) (2022).

[27] L. Lv, X. Wang, Q. Zhang, Y. Xiang, X. Wu, C. Huang, Investigation of vertical thermal stratification and stratified air conditioning load for large space with low-sidewall supply air based on vertical temperature node model, J. Build. Eng. 69 (November 2022) (2023) 106297, https://doi.org/10.1016/j.jobe.2023.106297.

[28] X. Wang, et al., Prediction of vertical thermal stratification of large space buildings based on Block-Gebhart model: case studies of three typical hybrid ventilation scenarios, J. Build. Eng. 41 (September 2020) (2021), https://doi.org/10.1016/j.jobe.2021.102452.

[29] J. Hu, Y. Kang, J. Yu, K. Zhong, Numerical study on thermal stratification for impinging jet ventilation system in office buildings, Build. Environ. 196 (March) (2021) 107798, https://doi.org/10.1016/j.buildenv.2021.107798.

[30] M. Maivel, A. Ferrantelli, J. Kurnitski, Experimental determination of radiator, underfloor and air heating emission losses due to stratification and operative temperature variations, Energy Build. 166 (2018) 220–228, https://doi.org/10.1016/j.enbuild.2018.01.061.

[31] J. Li, et al., Comparative studies and optimizations of air distribution of underground building ventilation systems based on response surface methodology: a case study, J. Build. Eng. 75 (April) (2023) 106952, https://doi.org/10.1016/j.jobe.2023.106952.

[32] L. Kudela, M. Špiláček, J. Pospíšil, Multicomponent numerical model for heat pump control with low-temperature heat storage: a benchmark in the conditions of Central Europe, J. Build. Eng. 66 (September 2022) (2023), https://doi.org/10.1016/j.jobe.2023.105829.

[33] S. Rahnama, G. Hultmark, K. Rupnik, P. Vogler-Finck, A. Afshari, Control logic for a novel HVAC system providing room-based indoor climate control in residential buildings, J. Build. Eng. 65 (November 2022) (2023) 105766, https://doi.org/10.1016/j.jobe.2022.105766.

[34] J. Bursill, W. O'Brien, I. Beausoleil-Morrison, Proxy zone-level energy use estimation in a commercial building with a variable air volume system, J. Build. Eng. 33 (December 2019) (2021) 101498, https://doi.org/10.1016/j.jobe.2020.101498.

[35] Z. Xiong, J. Berquist, H.B. Gunay, C.A. Cruickshank, An inquiry into the use of indoor CO_2 and humidity ratio trend data with inverse modelling to estimate air infiltration, Build. Environ. 206 (June) (2021) 108365, https://doi.org/10.1016/j.buildenv.2021.108365.

[36] M.M. Andamon, P. Rajagopalan, J. Woo, Evaluation of ventilation in Australian school classrooms using long-term indoor CO_2 concentration measurements, Build. Environ. 237 (April) (2023) 110313, https://doi.org/10.1016/j.buildenv.2023.110313.

[37] X. Liu, X. Liu, T. Zhang, Influence of air-conditioning systems on buoyancy driven air infiltration in large space buildings: a case study of a railway station, Energy Build. 210 (2020) 109781, https://doi.org/10.1016/j.enbuild.2020.109781.

[38] S. Wei, P.W. Tien, T.W. Chow, Y. Wu, J.K. Calautit, Deep learning and computer vision based occupancy CO_2 level prediction for demand-controlled ventilation (DCV), J. Build. Eng. 56 (May) (2022) 104715, https://doi.org/10.1016/j.jobe.2022.104715.

[39] A. Franco, F. Leccese, Measurement of CO_2 concentration for occupancy estimation in educational buildings with energy efficiency purposes, J. Build. Eng. 32 (August) (2020) 101714, https://doi.org/10.1016/j.jobe.2020.101714.

[40] W. Fornari, G. Grozman, N. Wikström, P. Sahlin, Development of a BLOCK zonal model in a BPS software to predict thermal stratification and air flows, Energy Build. 294 (February) (2023) 113230, https://doi.org/10.1016/j.enbuild.2023.113230.

[41] B. Dai, Y. Tong, Q. Hu, Z. Chen, Characteristics of Thermal Strati Fi Cation and its Effects on HVAC Energy Consumption for an Atrium Building in South China, vol. 249, 2022, https://doi.org/10.1016/j.energy.2022.123425.

[42] B. Ho, B. Seo, S. Hyup, S. Yeon, K. Ho, Influences of different operational configurations on combined effects of room air stratification and thermal decay in UFAD system, Energy Build. 176 (2018) 262–274, https://doi.org/10.1016/j.enbuild.2018.07.015.

[43] K. Kovac, M. Kovacova, CFD Simulation of Air Temperature stratification in historical building of theatre, in: 19th International Multidisciplinary Scientific GeoConference SGEM 2019, vol. 19, 2019, pp. 411–416. Bulgaria.

[44] C. Porras-Amores, F.R. Mazarrón, I. Cañas, P. Villoría Sáez, Natural ventilation analysis in an underground construction: CFD simulation and experimental validation, Tunn. Undergr. Space Technol. 90 (March) (2019) 162–173, https://doi.org/10.1016/j.tust.2019.04.023.

[45] Comsol, "Buoyancy Flow in Water," no. 10 cm, pp. 1–34.

[46] G.E.B. Malomar, C. Mbow, P.D. Tall, A. Gueye, V.B. Traore, A.C. Beye, Numerical study of 2-D natural convection in a square porous cavity: effect of three mode heating, Open J. Fluid Dynam. 7 (1) (2017) 89–104, https://doi.org/10.4236/ojfd.2017.71007.

[47] COMSOL, COMSOL Multiphysics Reference Manual, 2019, p. 1742 [Online]. Available: www.comsol.com.

[48] D. Chen, Periodically reversible supply/exhaust ventilation strategy, Build. Environ. 46 (12) (2011) 2590–2597, https://doi.org/10.1016/j. buildenv.2011.06.014.

[49] UNI EN ISO 10 211: thermal bridges in buildings construction – heat flows and surface temperatures – detailed calculations. Annex C: Validation of calculation methods.